Oil & Gas Science and Technology – Rev. IFP, Vol. 60 (2005), No. 1, pp. 161-175

IFP International Workshop
Rencontres scientifiques de l'IFP

Gas-Water-Rock Interactions ... / Interactions gaz-eau-roche ...

Large-Scale Column Experiment: Study of CO_2,Porewater, Rock Reactions and Model Test Case

K. Bateman[1], G. Turner[1], J.M. Pearce[1], D.J. Noy[1], D. Birchall[1] and C.A. Rochelle[1]

1 British Geological Survey, Kingsley Dunham Centre, Keyworth, Nottingham NG12 5GG - United Kingdom
e-mail: kba@bgs.ac.uk - ght@bgs.ac.uk - jmpe@bgs.ac.uk - djn@bgs.ac.uk - dbirch@bgs.ac.uk - caro@bgs.ac.uk

Résumé — Expérimentation de longue durée sur grandes colonnes, dans le contexte du stockage géologique de CO_2 : étude des interactions eau-roche et modélisation — Au cours des opérations de stockage du CO_2 en aquifère profond, le gaz acide injecté peut être piégé de trois manières :

– en phase constituée, généralement un gaz surcritique (piégeage physique) ;

– dissous dans l'eau interstitielle (piégeage hydrodynamique) ;

– précipité sous forme de carbonates comme la calcite (piégeage minéralogique). La présente étude est consacrée aux réactions entre CO_2, l'eau interstitielle et la roche hôte.

Le but de ce travail est de fournir une expérience de laboratoire suffisamment bien contrainte, d'une durée assez longue (plusieurs mois), mettant en jeu des quantités connues de minéraux et de solution aqueuse enrichie en CO_2, dans des conditions aptes à représenter une situation réelle de stockage. Une telle expérience est susceptible de devenir un cas test pour valider une approche de modélisation géochimique à vocation prédictive, qui s'inscrit dans l'effort entrepris pour mieux comprendre le sort, à long terme, du gaz acide injecté dans le sous-sol.

L'expérience décrite, malgré son dispositif complexe, a fonctionné pendant une période de 7,5 mois. Des échantillons de fluide ont été régulièrement collectés, pour offrir un suivi des espèces dissoutes. Le matériel soumis à la réaction a pu ensuite être étudié, de manière à observer d'éventuels changements de composition minérale. Des modifications sensibles ont été mises en évidence sur les phases carbonatées, en accord avec les mesures effectuées sur l'effluent. À l'inverse, quoique des changements de silice dissoute aient été enregistrés, aucune manifestation tangible d'une altération des phases siliceuses n'a pu être révélée.

La modélisation des interactions eau-minéraux a pu être effectuée à l'aide du logiciel Precip, du *BGS*. En première approche, le modèle tend à surestimer l'intensité des réactions. La précipitation de certaines phases minérales, comme la dawsonite, est prédite en quantités substantielles, alors qu'il n'y en a pas de trace visible dans le matériel expérimental.

Les différences entre réalité et modèle montrent le besoin de meilleures données, tant thermodynamiques que cinétiques, dans les conditions pertinentes pour le stockage de CO_2 (pH, température, pression, composition des eaux de formation). On ne peut se contenter d'extrapolations.

Abstract — Large-Scale Column Experiment: Study of CO_2, Porewater, Rock Reactions and Model Test Case *— During underground carbon dioxide (CO_2) storage operations in deep reservoirs, the CO_2 can be trapped in three ways;*

- *as "free" CO_2, most likely as a supercritical phase (physical trapping);*
- *dissolved in formation water (hydrodynamic trapping);*
- *precipitated in carbonate phases such as calcite (mineral trapping). This study focuses on the reactions between CO_2, porewater and host rock.*

The aim of this work was to provide a well-constrained long-term laboratory experiment reacting known quantities of minerals with CO_2-rich fluids, in order to try and represent situations where CO_2 is being injected into lithologies deep underground. The experimental results can then be used as a test case with which to help validate predictive geochemical computer models. These will help improve our ability to predict the long-term fate of carbon dioxide (CO_2) stored underground.

The experiment, though complex in terms of equipment, ran for approximately 7.5 months. The reacted material was then examined for mineralogical changes and the collected fluids analysed to provide data on the fate of the dissolved species. Changes were readily observable on the carbonates present in the starting material, which matches well with the observed trends in the fluid chemistry. However, although changes in silica concentrations were seen in the fluid chemistry no evidence for pitting or etching was noted in the silica bearing phases.

Modelling of the experimental systems was performed using the BGS coupled code, PRECIP. As a general conclusion, the model predictions tend to over estimate the degree of reaction compared with the results from the experiment. In particular, some mineral phases (e.g. dawsonite) that are predicted to form in large quantities by the model are not seen at all in the experimental system.

The differences between the model predictions and the experimental observations highlight the need for thermodynamic and kinetic data to be available under appropriate conditions (pH, and chemical composition of the fluid as well as temperature, and pressure), as extrapolation or "best guesses" may lead to errors being induced in the predictions. These errors and gaps in the data become obvious when comparing model predictions with experiments which serves to emphasise the importance of having "test cases" with which the models can be validated.

INTRODUCTION

During underground carbon dioxide (CO_2) storage operations in deep reservoirs, the CO_2 can be trapped in three ways; as "free" CO_2, most likely as a supercritical phase (physical trapping); dissolved in formation water (hydrodynamic trapping); precipitated in carbonate phases such as calcite (mineral trapping).

During the early stages of storage, "physical trapping" is likely to be most important trapping mechanism. However, over time, hydrodynamic trapping and eventually mineral trapping will make significant contributions to the long-term containment of CO_2. This study focuses on the reactions between CO_2, porewater and host rock.

The aim of this work was to provide a well-constrained long-term laboratory experiment reacting known quantities of minerals with CO_2-rich fluids, order to try and represent situations where CO_2 is being injected into lithologies deep underground. The experimental results can then be used as a test case with which to help validate predictive geochemical computer models. These will help improve our ability to predict the long-term fate of carbon dioxide (CO_2) stored underground.

Within an underground CO_2 storage operation there will be a region of free CO_2 (*e.g.* the CO_2 "bubble") overlying original formation porewater. The CO_2 will dissolve into the formation water at a rate controlled by factors such as: the rate of CO_2 injection, the rate of CO_2 dissolution into the porewater, the chemistry of the porewater, the surface area available for reaction, and the rate of diffusion of the CO_2 into the porewater away from the porewater-CO_2 interface. Therefore, in different parts of the formation there will exist porewaters with a range of dissolved CO_2 concentrations. Within an experimental programme, it is not possible to simulate all possible dissolved CO_2 concentrations, so the "CO_2-saturated" case where maximum CO_2 is dissolved into the porewater was chosen, since it is anticipated that maximising aqueous CO_2 concentrations will maximise the degree of fluid-rock reaction and provide a "limiting case" for study. The experiment was conducted within The *Hydrothermal Laboratory of the British Geological Survey*, Keyworth, United Kingdom.

1 EXPERIMENTAL SETUP

1.1 Equipment

Prior to performing the experiments, it was necessary to design and construct equipment that would perform well.

Although dry supercritical CO_2 is relatively inert, in the presence of water or saline solution it is much more reactive. Previous studies (Schremp and Roberson, 1975) have shown that steel will corrode and standard O-ring seals will blister and fail. To minimise both corrosion and experimental failure, exposed surfaces were chosen so as to be as inert as practicable. Therefore, the wetted parts of the stainless steel vessels (steel types 316 and EN54) were generally lined with PTFE (polytetrafluoroethylene), the high pressure tubing was made of either 316 stainless steel or PEEK™ (polyetheretherketone), and pressurised fluid sampling containers were constructed entirely from titanium.

A simplified of the complete experimental system is shown in Figure 1 and a photograph of the main pressure vessel and associated pumps is shown in Figure 2. Essentially, the equipment consists of a column 100 cm long, with an internal diameter of 3.6 cm containing the packed reacting mineral assemblage. This column is contained inside a large heated pressure vessel, with the confining pressure being maintained by a syringe pump. The experiment was initially raised to a pressure of 100 bar using a regulator and a 130 bar pressure CO_2 cylinder (*Air Products Inc.*). The CO_2 pressure was maintained at 100 bar throughout the experiment using a syringe pump. The reactant fluid was equilibrated with CO_2 at a temperature of 70ºC and a pressure of 100 bar, before being displaced by the pressurising CO_2. Fluid flow out of the column was controlled by the third syringe pump. Samples of the reactant fluid were collected using a 30 ml capacity, titanium floating piston pressure sampler. Two conditioning vessels were used, with one supplying fluid to the column and the other being used to equilibrate the reactant fluid with CO_2 under the experimental conditions.

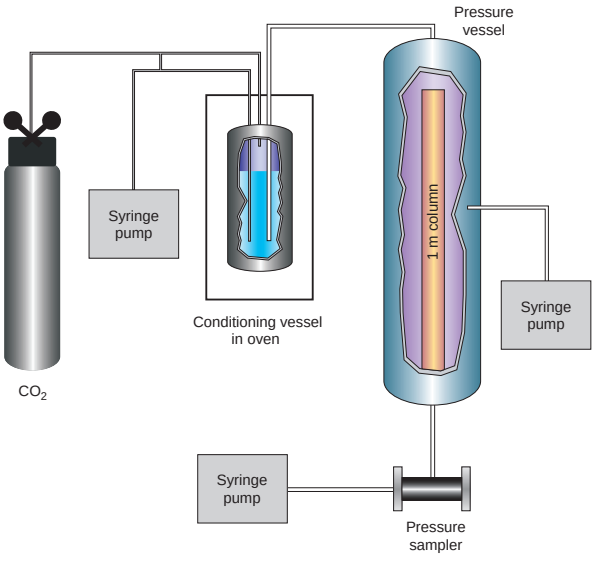

Figure 1

Simplified schematic of equipment.

Figure 2

Photograph showing pressure vessel, pumps and sampling vessels.

1.2 Starting Materials

The starting materials were chosen to be similar to that of the saline aquifer CO_2 storage (SACS) project (Pearce *et al.*, 2000), so that results could be compared with experiments previously conducted. Thus the reacting fluid was identical to that used in the SACS batch and flow experiments; Table 1 gives the chemical composition of the fluid prior to equilibration with CO_2. The fluid was prepared in one batch from laboratory grade reagents.

The starting minerals, apart from quartz, were prepared from individual mineral specimens that were crushed and sieved to 125-250 μm. The quartz was prepared from a pre-crushed material (supplied by *Sigma-Aldrich*). Table 1 gives details of the mixture composition, this was based on that of the Utsira sand previously analysed as part of the SACS project. The Utsira Formation (Pearce *et al.*, 2000) comprises predominant quartz with minor plagioclase, K-feldspar, calcite and common bioclastic debris. Some detrital grains are covered by a thin clay coating of mainly smectite with minor illite and chlorite. A synthetic mixture was used since this allowed complete control over which minerals were present in the mixture and also allowed the surface areas to be determined (by N_2 BET) for the separate minerals as well as the combined mixture.

TABLE 1

Starting materials

Synthetic formation fluid (prior to equilibration with CO_2)			Synthetic mineral composition		
pH	7.1 (at 20°C) Concentration ppm	mol·dm^{-3}	Phase	Surface area m^2 g^{-1}	Weight (%)
Na	10392	4.52×10^{-1}	Quartz	0.06	80
K	208	5.32×10^{-3}	Labradorite	0.1	10
Ca	426	1.06×10^{-2}	K-feldspar	0.08	1
Mg	630	2.59×10^{-2}	Albite	0.1	2
Sr	10	1.14×10^{-4}	Calcite	0.07	3
Ba	0.5	3.64×10^{-6}	Dolomite	0.08	1
Fe	2	3.58×10^{-5}	Muscovite	1.62	2
Cl	18482	5.21×10^{-1}	Chlorite	0.75	1
HCO_3	707	1.16×10^{-2}	Mixture	0.12	100

2 ANALYTICAL METHODS

2.1 Fluid Samples

Samples of the reactant fluid were collected using a titanium floating piston pressure sampler. The reacted fluid was then rapidly depressurised before being prepared for chemical analysis. Samples of the unreacted and reacted fluids were split into several sub-samples. A sub-sample of 1 ml was taken for immediate analysis of pH. Measurements of pH were made using an Orion® 900A pH meter calibrated using Whatman® NBS traceable buffers at pH 4, 7, and 10, all measurements were performed at 20°C.

Another sub-sample was taken using a polythene syringe and filtered using a 0.2 µm "Anotop"® nylon syringe filter. A 10 ml aliquot of this sample was pipetted into a polystyrene tube and acidified with 0.1 ml of concentrated "Aristar"® nitric acid. This sample was analysed subsequently for major and trace cations by inductively coupled plasma-optical emission spectroscopy (ICP-OES). A further aliquot of the filtered sample (approximately 4 ml) was also taken and placed in a polyethylene tube for analysis of anions by ion chromatography (IC). All fluid samples were stored in a fridge (at about 5°C) prior to analysis.

2.2 Analytical Techniques for Solids

2.2.1 Scanning Electron Microscopy

To ensure representivity, samples for scanning electron microscopy (SEM) were separated by riffle splitting at specific intervals. Each subsample was sprinkled onto an Al pin-type stub. Cementing grains with a carbon-based glue ensured electrical contact. All specimens were then coated in a 25 nm layer of carbon by evaporation in an Edwards 306A carbon coater.

Specimens were examined in both secondary and backscattered mode in a Leo 435 VP scanning electron microscope at an operating voltage of 20 kV. Mineral identification was aided by an Oxford Instruments Isis energy dispersive X-ray microanalysis system.

2.2.2 BET/Nitrogen Surface Area Analysis

Surface area analyses were also undertaken using the single-point BET/N_2 method (Brunauer *et al.*, 1938) based on the quantity of gas that adsorbs as a single layer of molecules on a solid surface. Approximately 1 g of each sample was loaded into a glass sample tube and heated at 60ºC overnight in a vacuum oven. Immediately preceding surface area analysis, the samples were degassed for a further 30 min on the degassing station of the Micromeritics FlowSorb II 2300 surface area analyser. A mixture of 30% N_2/70% He was used as a gas supply and analyses were carried out at atmospheric pressure and at liquid N_2 temperature. The manufacturers claim analyses are typically better than ±3% accuracy and within ± 0.5% reproducibility for materials of low surface area.

3 RESULTS

The experiment was undertaken using a column 100 cm long and with an internal diameter of 3.6 cm. The initial total weight of the synthetic mineral mixture was 1604 g, great care was taken when filling the column to ensure homogeneity. The initial porosity of the column was determined (by the difference between the dry and wet weights of the column, corrected for density) to be 39.5%. The reactant fluid was equilibrated with CO_2 at a temperature of 70ºC and a pressure of 100 bar, before being pumped into the column held under the same conditions. Fluid was passed along the column at a constant flow rate of 1.25 cm^3·h^{-1} for 5510 h (approximately 7.5 months).

Fluid samples were collected using the titanium pressure sampler, at intervals throughout the duration of the experiment, the fluids were depressurised/discharged from the titanium pressure samplers and preserved using the methods described above.

3.1 Preparation of Experimental Products

On completion of the column experiment, the entire column assembly was flushed (under experimental conditions, 70ºC, 100 bar,) with isopropyl alcohol—in order to displace the reacting fluid. This was performed in order to try to minimise salt formation when the column was dried and prepared for mineralogical analysis (previous experience has shown that failure to do so may obscure observations of subtle

mineralogical features). Once the flushing was complete and the column depressurised and returned to laboratory temperature and pressure, it was divided into 2.5 cm intervals. An additional split was also taken from the very beginning of the column (0.0-0.3 cm). Each split was air-dried.

3.2 Mineralogical Investigations

The unreacted starting material comprises well sorted, clean, angular to well-rounded quartz grains with some angular faces, angular feldspar grains, mica grains and blocky to angular, irregular calcite and dolomite grains (*Fig. 3*, *Table 1*). All grain surfaces are fresh with no evidence for pitting or etching.

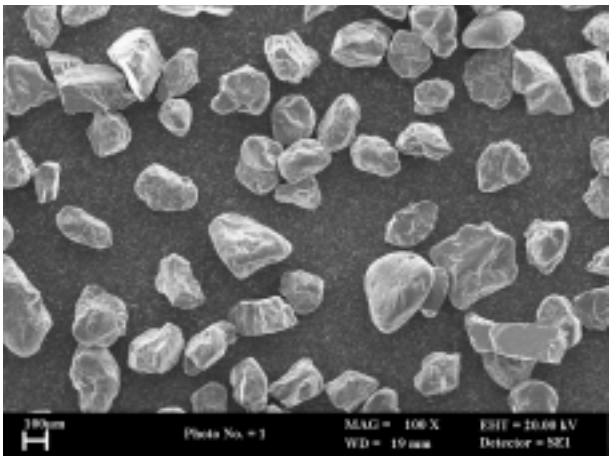

Figure 3

Typical view of unreacted starting material with no evidence for etching on carbonate grains.

Results of the mineralogical investigations are summarised in Figure 4. At the beginning of the column, a reduction in the proportions of calcite and dolomite indicates that significant dissolution of these components has occurred. Where present, dolomite grains are typically severely corroded (*Fig. 4*, plate 1). The proportion of calcite and dolomite is reduced from the beginning of the column for approximately 10 cm. Between 10 and 20 cm, the proportions of original calcite and dolomite grains return to those present in the unreacted starting material. After 20 cm, carbonate grains are more typically fresh with no evidence for surface etching.

In addition to the dissolution of carbonate grains at the inlet end of the column, there is also some limited evidence for traces of dolomite precipitating. This dolomite, which partially blocks pore-throats and locally cements some grains, is only developed in the first interval sampled (*Fig. 4*, plate 2), 0.3-2.5 cm.

A pink colouration was noted on the exposed surfaces of some of the sawn samples. This was sampled separately and was found to contain minor, micron-scale, irregular iron oxide particles that form discrete patchy coatings on some grains. These patches were present from the column inlet to approximately 5 cm (*Fig. 4*, plate 3). The source of this iron may be breakdown of Fe-rich dolomite. However, it is felt more likely that this may represent contamination from parts of the equipment itself.

Surface Area Analyses

Surface area values for both unreacted and reacted samples are very low, naturally reflecting the low surface areas of the component minerals (*Table 2*) and (*Fig. 5*). The unreacted sample has a surface area of 0.1 m^2g^{-1} (± 0.01 m^2g^{-1}, the standard deviation from three repeat measurements on the same sample), which is the same as the manufacturer's quoted detection limit. Although the instrument is capable of determining surface areas below 0.1 m^2g^{-1}, accurate results (with quoted ± 3% instrumental error) can only be obtained for values above this limit.

However, despite very low surface areas that are close to the detection limit, there appears to be a trend that may reflect the corrosion observed at the beginning of the column (*Fig. 5*). At the inlet end of the column, the surface area increases to 0.14 ± 0.01 m^2g^{-1} and at the halfway point, decreases to 0.12 ± 0.01 m^2g^{-1} and at the end of the column the surface area decreases to 0.08 m^2g^{-1}. Assuming no dissolution or precipitation has occurred at the halfway point or end of the column, the values for these intervals can be taken to represent the natural variability in surface areas between different subsamples, *i.e.* the precision in the results as opposed to instrumental accuracy. This would increase the errors quoted above, from the standard deviations derived from 3 (or 4) repeat measurements on the same sample, to a value of 0.02 m^2g^{-1}. Nevertheless, this still gives confidence that the surface area at the inlet end of the column is still higher than the unreacted starting material and those of the other reacted samples, which should be considered to be the same value within an error of 0.02 m^2g^{-1}. This represents an increase in surface area of between 17 and 20%.

3.3 Chemistry

On completion of the experiment all of the collected fluids were analysed using ICP and IC, the data set is shown in Table 3 and selected components (Ca, Mg and SiO_2) in Figure 5.

The pH of the unequilibrated fluid is ≈ 7.1. The initial pH of the equilibrated fluid pH ≈ 5.1, which rises to pH ≈ 6.6 during the first 300 h of reaction before falling to pH ≈ 6.2 after 1500 h reaction. The pH then remains at pH ≈ 6.2 for the remainder of the duration of the experiment. These changes in pH are consistent with the removal/reaction of CO_2 from the reactant fluid.

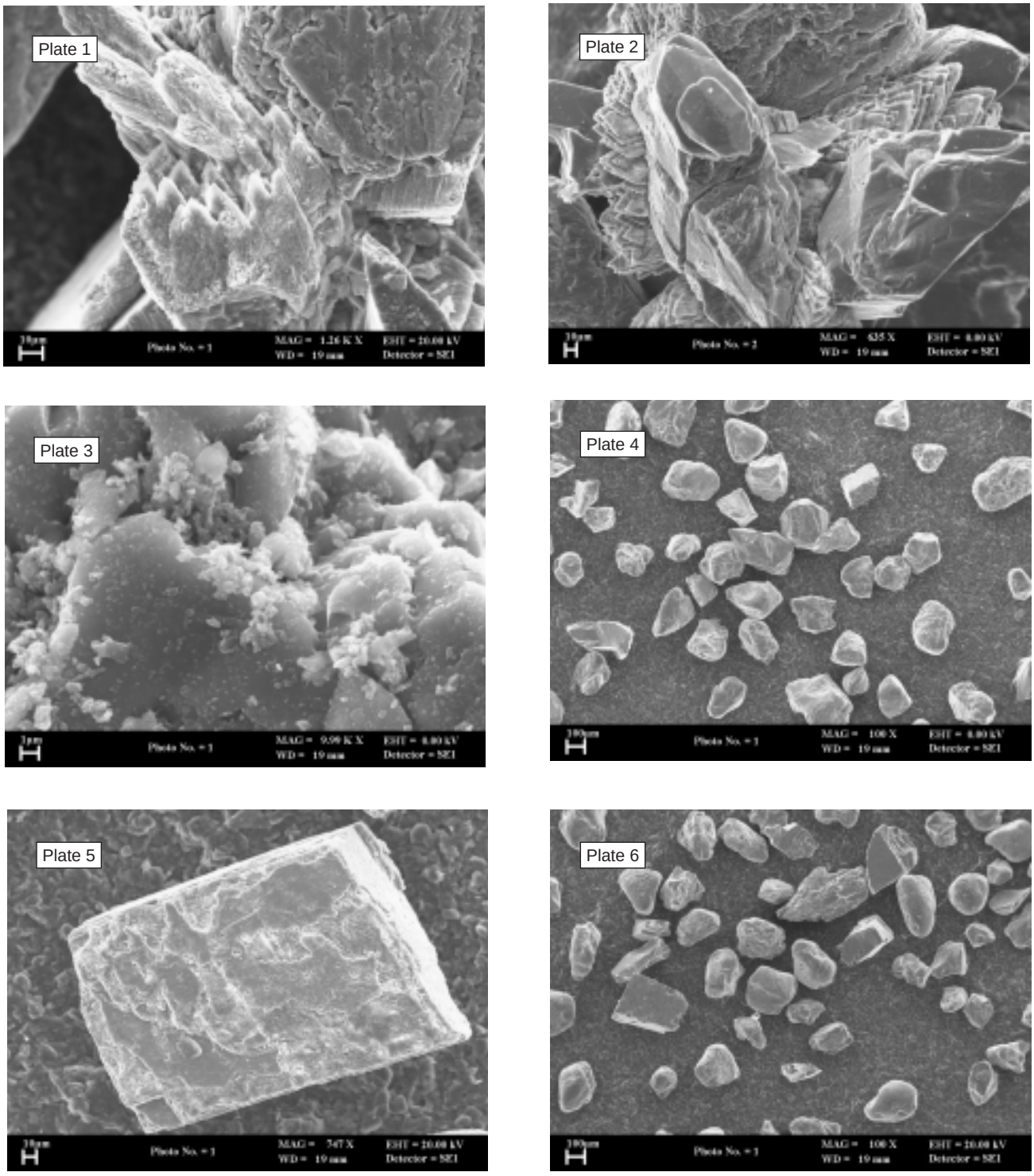

Figure 4

SEM photographs of reacted material.

Plate 1: 0-0.3 cm from inlet, dolomite and calcite grains showing severe corrosion.

Plate 2: 0.3-2.5 cm from inlet, traces of secondary dolomite, partially blocking pore-throats and locally cementing grains together.

Plate 3: 2.5-5.0 cm from inlet, minor iron oxides form patchy discrete coatings on some grains.

Plates 4 and 5: corrosion of calcite and dolomite grains from the beginning of the column.

Plate 6: 30 cm from inlet, no evidence for corrosion; all grains appear as fresh as in the starting material.

For most of the experiment, there is little change in the concentration of sodium and chloride from the relatively high starting values. Two abrupt drops in concentration are observed at approximately 300 and 3200 h reaction but these are related to equipment/operational problems, and are not thought due to any chemical reactions taking place. Potassium similarly shows little change in concentration during the experiment.

Aluminium concentrations throughout the experiment were close to or below that of the ICP detection limit. Some data was obtained in the early stages of the experiment and where this data exists, the Al concentrations are higher than starting values. This suggests some limited evidence for dissolution of an Al bearing phase.

TABLE 2

Surface area analyses (BET N_2) for selected intervals

	Unreacted sample	**Sample 1**	**Sample 19**	**Sample 37**
Distance from inlet		0.3-2.5 cm	45.0-47.5 cm	90.0-92.5 cm
1st measure	0.1	0.15	0.12	0.08
2nd measure	0.09	0.14	0.11	0.08
3rd measure	0.1	0.13	0.12	0.08
4th measure		0.14		
mean	0.10	0.14	0.12	0.08
Standard deviation (s.d.)	0.006	0.008	0.006	0.000

Units = $m^2 \cdot g^{-1}$

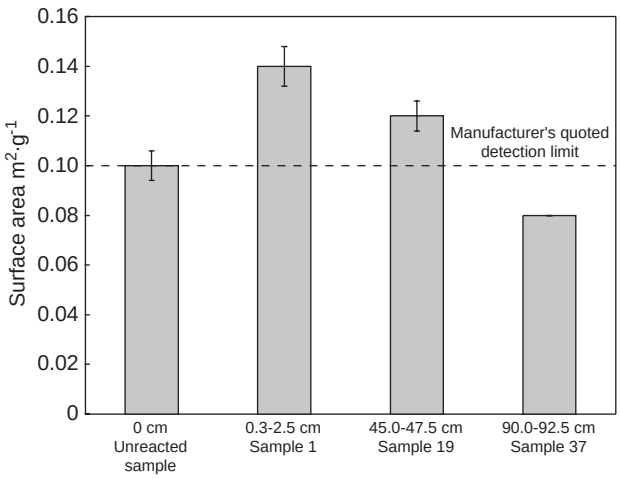

Figure 5

BET N_2 mean surface areas for starting material and reacted intervals down the column. Error bars are calculated standard deviations from the mean result.

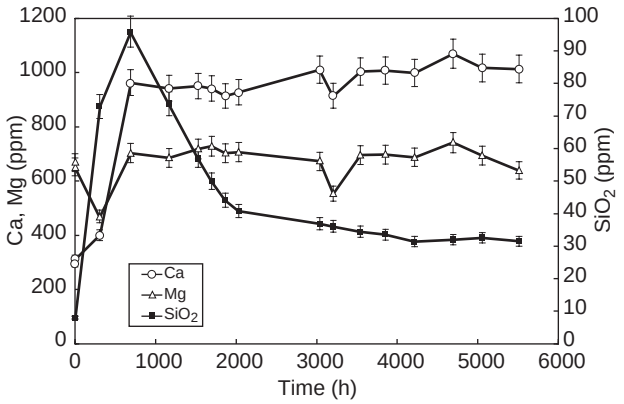

Figure 6

Ca, Mg and SiO_2 concentrations with time.

Both iron and manganese show real increases in concentration from that of the unreacted fluid but there is no obvious trend in the data. It is thought that one of the main sources for the increased values of these elements in the reacted fluids is possibly the stainless steel used experimental equipment. This is consistent with the mineralogical analysis in which iron oxide particles with a pink colouration were noted on the exposed surfaces of some of the sawn samples.

The concentration of calcium in solution shows a large increase in the first 700 h of reaction from a starting value of 298 $mg \cdot kg^{-1}$ to ≈ 960 $mg \cdot kg^{-1}$. There then follows a slower rise in concentration to ≈ 1000 $mg \cdot kg^{-1}$ at approximately 3000 h of reaction. For the reminder of the experiment the concentration calcium in solution remains close to this level.

Magnesium, (*Fig. 6, Table 3*) shows a similar trend to that of calcium though the increases are not as great, from 668 $mg \cdot kg^{-1}$ in the unreacted fluid to ≈ 700 $mg \cdot kg^{-1}$ later in the experiment.

These increases in calcium and magnesium concentrations in the fluid are consistent with the mineralogical observation, which noted that there was dissolution of calcite and dolomite.

The results for silica (*Fig. 6, Table 3*) show a slightly different behaviour in that although the concentration rises sharply in the first 700 h of reaction from a starting value of 8 (SiO_2) $mg \cdot kg^{-1}$ to ≈ 96 (SiO_2) $mg \cdot kg^{-1}$. There then follows a decrease in concentration over the next 2000 h of reaction to ≈ 34 (SiO_2) $mg \cdot kg^{-1}$. The concentration of silica remains close to this value for the remainder of the experiment. The initial rapid increases in silica concentration may be the result of preferential dissolution of fines produced during the sample preparation. The later reduced levels of silica may therefore be more representative of the behaviour of the mineral assemblage. The source of this dissolved silica is not

TABLE 3
Fluid chemistry analytical data (ppm)

Sample code	1000/blk	1000/1	1000/2	1000/3	1000/4	1000/5	1000/6	1000/7	1000/8	1000/9	1000/10	1000/11	1000/12	1000/13	1000/14	1000/15
Time (h)	0.0	305.8	689.5	1168.6	1528.2	1697.3	1865.3	2032.7	3037.9	3206.9	3542.6	3854.2	4214.7	4694.7	5054.5	5510.1
Pressure (bar)	-	100.0	100.0	100.0	100.0	100.0	100.0	100.0	100.0	100.0	100.0	100.0	100.0	100.0	100.0	100.0
pH (at 20°C)	5.08	6.56	5.98	6.30	6.19	6.21	6.20	6.08	6.14	6.08	6.09	6.20	6.20	6.17	6.20	6.14
Ca	298	401	963	942	950	941	914	927	1010	915	1004	1008	999	1070	1017	1013
Mg	668	469	703	686	718	729	703	706	673	553	695	698	688	742	694	639
Na	11611	7620	11437	11306	11622	11735	11413	11417	11104	8840	11105	10997	10875	11926	11374	10888
K	248	223	252	238	248	253	247	253	245	189	242	241	244	253	249	241
HCO_3	100	561	1030	1080	1200	1100	1120	1180	1440	1430	1620	1400	1750	2180	2400	2320
Cl^-	18942	13326	19418	19067	20905	19791	19574	18964	18582	15578	18847	19288	19073	22380	19285	19528
Si	<3.75	34.1	44.8	34.5	26.6	23.4	20.6	19.1	17.2	16.9	16.1	15.7	14.7	15.0	15.2	14.7
SiO_2	8.02	72.9	95.9	73.7	57.0	50.0	44.1	40.8	36.9	36.1	34.4	33.5	31.4	32.0	32.6	31.5
Ba	0.416	0.998	0.699	1.22	0.752	0.690	0.590	0.584	0.780	0.502	0.605	0.762	0.941	0.787	1.66	0.717
Sr	5.39	4.01	5.90	6.88	7.08	7.19	7.62	7.80	8.07	6.05	6.95	6.57	7.11	7.22	6.64	6.76
Mn	<0.100	0.872	0.145	0.371	0.339	0.343	0.459	0.377	0.404	0.510	0.409	0.371	0.324	0.308	1.04	1.12
Fe	3.44	6.60	2.50	26.6	27.5	28.5	14.8	27.1	29.2	37.5	21.9	19.0	17.9	21.4	29.8	59.7
Al	<0.050	1.29	0.108	0.591	0.709	0.053	<0.050	<0.050	<0.050	0.156	<0.050	0.143	<0.050	<0.050	<0.050	<0.050
Ni	0.311	0.211	0.162	0.634	0.659	0.818	1.53	1.14	0.630	0.584	0.631	0.490	0.484	0.872	7.00	17.4
Zn	<0.250	0.327	<0.250	2.20	1.27	0.587	<0.250	0.284	2.55	3.02	2.11	1.54	0.801	0.641	<0.250	1.37

1000/blk represents the sample blank (unreacted, equilibrated fluid),
1000/X represents fluid sample X.
< represents concentration below quoted detection limit

clear from the mineralogical analysis as no obvious signs of dissolution were seen on the silica bearing phases. Possible phases are the quartz, feldspars, muscovite and chlorite present in the initial material.

The bicarbonate concentrations are seen to be increasing over time, with concentrations of approximately 2400 mg/l by the end of the experiment. It is worth noting that all the samples were analysed at the end of the experiment, and therefore early samples may have reequilibrated with the air in the sample container (reducing bicarbonate concentrations). Consequently, later samples are more likely to be closer to *in situ* values.

4 PREDICTIVE MODELLING

Predictive model calculations of the interaction of a CO_2 saturated fluid with the minerals of a column of synthetic reservoir rock were undertaken to simulate the progress of the experiment using the BGS coupled code, PRECIP (Noy, 1998; Savage, 2002). This code couples fluid flow and fluid/rock reaction in a computationally efficient manner. It was also specifically designed to incorporate reaction kinetics, which is vital to address when considering non-equilibrium systems. The chemical equilibrium and kinetic constants were taken from literature, previous experience, or approximated as necessary.

PRECIP was developed to examine changes in the mass-transfer properties of a system resulting from mineral reactions. A full description of PRECIP may be found in Savage (2002) a brief summary is given here. The conceptual approach of PRECIP is of a one-dimensional flow path along which fluid flow is Darcian and on which precipitation and dissolution reactions can take place amongst a number of components. The flow field is defined by either fixed head values at each end of the path or by a specified flow rate along it. The chemical reactions are described by kinetic rate laws and the aqueous components are transported by advection, diffusion and dispersion. As the chemical reactions proceed, the masses of precipitates change at each point on the path with consequent changes in the porosity. These porosity changes may be related to changes of permeability by a user-defined function, thereby affecting the flow field. The transport and reaction equations are fully coupled and solved simultaneously. PRECIP uses mineral masses as variables so the rate equations have been written in terms of change of mineral mass. Transition state theory *(e.g.* Helgeson *et al.*, 1984) can be used to derive a rate equation of the form:

$$\frac{\partial M_j}{\partial t} = a_j k_j \left(\Omega_j - 1\right)$$

where M_j is the mass concentration of mineral component j, in mol per unit volume of porous medium, a_j is the reactive surface area of mineral j per unit volume of porous medium, k_j is the dissolution rate constant. Ω_j is the saturation ratio given by;

$$\Omega_j = \frac{Q_j}{K_{eq}}$$

where Q_j is the ion activity product for the mineral, and K_{eq} is the thermodynamic equilibrium constant for the hydrolysis of the mineral.

By restricting the calculation to just the major aqueous components, the computing times are kept relatively short, allowing the use of refined grids and the simulation of long times.

4.1 Experimental Parameters

The parameters used in the model are listed in Table 4. For the modelling of the experiment the flow field was defined a specified flow rate along the column. In addition, coupling between porosity and permeability was not invoked due to the lack of data concerning the functional form and it was expected that any porosity changes were relatively minor.

TABLE 4

Precip parameters

Parameter	Value
Column length	100 cm
Column internal diameter	3.6 cm
Temperature	70ºC
Pressure	100 bar
Cross sectional area of column, A	1.018×10^{-3} m^2
Volume of column, V	1.018×10^{-3} m^3
Volume of fluid in column, V_f	4.021×10^{-4} m^3
Initial mass of minerals in column	1.604 kg
Flow rate of fluid down column, Q	3.472×10^{-10} m^{3}s^{-1}
Specific flow rate, q (= Q/A)	3.411×10^{-7} m s^{-1}
Porosity, ϕ	0.395
Flow velocity, v (= q/ϕ)	8.636×10^{-7} m s^{-1}
Longitudinal dispersity	1 cm
Transit time through column, $t_{transit}$	321.66 h
Experiment duration	17.130 pore volumes

4.2 Input Fluid Compositions

The composition of the synthetic formation fluid is given in Table 1. These components were speciated using the PHREEQC (Parkhurst and Appelo, 1999) code with the LLNL database to give the initial *in situ* fluid composition in terms of a selected set of basis species as shown in Table 5. This fluid was then allowed to equilibrate with CO_2 at 100 bar pressure, again using the PHREEQC code, to give the composition of the input fluid shown in Table 5. It may be noted that Sr and Ba have been omitted from Table 5. This

was because they are only present at low concentrations and are not represented in any of the minerals of the initial column composition (see below). In addition to the basis species listed in Table 4, eleven aqueous complexes were included in the model. Their dissociation reactions and equilibrium constants are given in Table 6

4.3 Initial Mineral Composition

The initial composition of the minerals used to make up the column is given in Table 1. For the purposes of modelling, labradorite is considered to be a mixture of equal parts of anorthite and albite whilst chlorite is a mixture of clinochlore and daphnite.

In addition to this list of minerals, dawsonite and gibbsite were included in the model as potential extra secondary minerals. Also, a further 17 minerals were checked by the model for their saturation state during the course of the model's calculations. Table 7 lists all the minerals considered together with their chemical and kinetic constants.

TABLE 5

Chemical speciation of initial and input fluids

Component	Initial concentration ($mol \cdot dm^{-3}$)	Input concentration ($mol \cdot dm^{-3}$)
$Al(OH)_2^+$	0.0	0.0
Ca^{2+}	1.02×10^{-2}	1.02×10^{-2}
Cl^-	5.11×10^{-1}	5.11×10^{-1}
Fe^{2+}	1.69×10^{-5}	1.68×10^{-5}
H^+	1.01×10^{-7}	1.53×10^{-4}
HCO_3^-	8.64×10^{-3}	9.05×10^{-3}
K^+	5.41×10^{-3}	5.41×10^{-3}
Mg^{2+}	2.26×10^{-2}	2.26×10^{-2}
Na^+	4.43×10^{-1}	4.43×10^{-1}
SiO_2	0.0	0.0

TABLE 6

Aqueous complexes used in the model

Aqueous complex	Log *K*
$CaHCO_3^+ => Ca^{2+} + HCO_3^-$	–1.22
$CO_{2(aq)} + H_2O => HCO_3^- + H^+$	–6.30
$FeCl^+ => Fe^{2+} + Cl^-$	–0.0242
$MgCl^+ => Mg^{2+} + Cl^-$	–0.0044
$MgHCO_3^+ => Mg^{2+} + HCO_3^-$	–1.23
$NaCl => Na^+ + Cl^-$	0.606
$NaHCO^3 => Na^+ + HCO_3^-$	0.185
$AlOH^{2+} + H_2O => Al(OH)_2^+ + H^+$	–4.54
$Al^{3+} + 2\ H_2O => Al(OH)_2^+ + 2\ H^+$	–8.30
$AlO_2^- => Al(OH)_2^+ - 2\ H^+$	10.52
$HAlO_2 => Al(OH)_2^+ - H^+$	4.78

Data for the equilibrium constants used here have been taken from EQ36 database data0.com.V8.R6, which is also the source for llnl.dat used with PHREEQC. Data for the kinetic constants have been taken from Knauss and Wolery (1986, 1988, 1989), Brady and Walther (1989, 1990), and Rochelle and Coombs (pers comm.). However, these references are mainly concerned with high pH conditions so that some extrapolation has been necessary. In addition, no specific data were available for anorthite, K-feldspar, clinochlore, daphnite, dawsonite, or gibbsite so that it has been necessary to make guesses as to how these minerals behave relative to the better known ones. Finally, it has been found in previous columns studies (Hoch *et al.*, 2002) that literature dissolution rates are commonly too fast to be compatible with the results from such experiments, so some "rounding down" has been applied to the silicate mineral rates.

4.4 Modelling Results

It should be noted the results discussed below are "blind" predictions using the known experimental parameters and with data available from the literature with all calculations being performed prior to the results of the experiments being made available. This was performed to provide a better test of the predictive capability of the Precip.

The concentrations of all aqueous basis components in the outflow fluid are shown in Figure 7a where it can be seen that there are two periods when significant changes are occurring.

The first period of change is at around 3-400 h (*Fig. 7b*) and represents the breakthrough of the first pore volume of the input fluid. At around this time there are distinct rises in the concentration of Ca^{2+}, HCO_3^-, Mg^{2+}, H^+, and $Al(OH)_2^+$. In addition, the levels of Fe^{2+} and SiO_2 rise more gradually over the whole of the first 400 h. From about 500 h through to about 4500 h, the system appears to be in a steady condition after which time the second main phase of change is seen. Here, there are rises in the concentration of Mg^{2+}, H^+, and $Al(OH)_2^+$ together with reductions in concentration of Ca^{2+} and HCO_3^-.

The first set of changes is clearly the result of the arrival of the CO_2 saturated fluid at the outlet end of the column. To understand the cause of the second period of change it is necessary to examine the changes in the distribution of carbonate minerals by the end of the modelling. These are shown in Figure 8, where it can be seen that the calcite initially present in the column has been almost completely removed and replaced by dolomite. It is probable that the emergence of this calcite/dolomite reaction front that causes the second phase of changes in the outflow fluid chemistry.

Other minor changes to the mineral assemblage are calculated to have taken place during the experiment and these are plotted in Figure 9. Here is can be seen that dawsonite is predicted to form in very small amounts along most

Table 7

Minerals included in the model calculations together with the initial mass density and surface area used for each in the model, their equilibrium constants (log *K*) and kinetic dissolution rates (log *k*).

Mineral	**Mass density ($mol \cdot m^{-3}$)**	**Surface Area (m^{-2})**	**Log k**	**Log K ($mol \cdot m^{-2}s^{-1}$)**
Quartz	20981	75638	–3.37	–12.0
Anorthite	283	7879	19.4	–11.7
Albite	421	11031	1.23	–12.0
K-feldspar	57	1261	–1.18	–12.0
Calcite	472	3309	1.19	–7.0
Dolomite	85	1261	1.02	–7.0
Muscovite	79	51056	7.68	–14.0
Clinochlore	14	5909	53.1	–13.0
Daphnite	11	5909	40.2	–13.0
Dawsonite	0.0	16000	2.64	–7.0
Gibbsite	0.0	16000	5.37	–11.7
"Look-up" minerals				
Analcime			4.19	
Beidellite-Ca			1.48	
Beidellite-Mg			1.32	
Beidellite-Na			1.64	
Celadonite			5.33	
Chalcedony			–3.14	
Huntite			6.17	
Hydromagnesite			23.9	
Illite			4.68	
Kaolinite			3.12	
Laumontite			9.02	
Magnesite			1.23	
Montmor-Ca			–0.28	
Montmor-Mg			–0.44	
Montmor-Na			–0.12	
Siderite			–0.99	
Stilbite			–1.62	

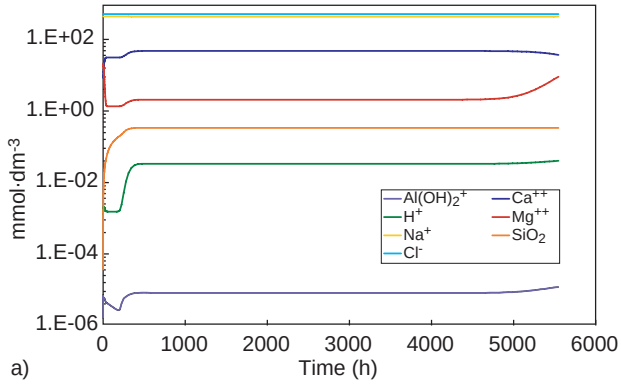

Figure 7a

Concentrations of basis species in the out-flowing fluid from the column as a function of time.

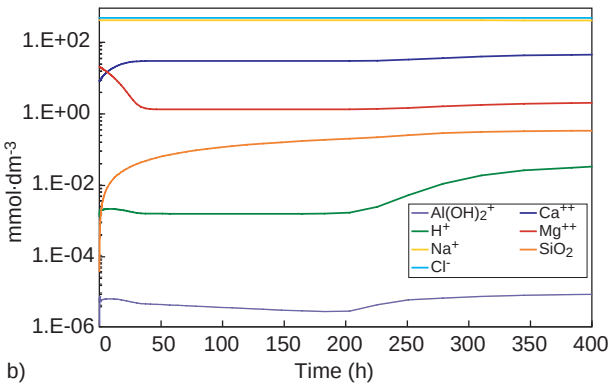

Figure 7b

Concentrations of basis species in the out-flowing fluid from the column as a function of time, over first 500 h.

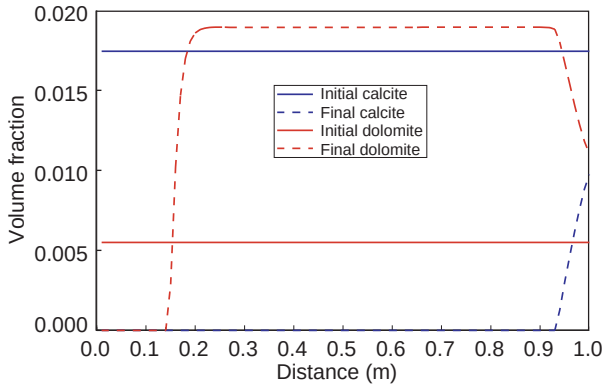

Figure 8

Calculated profiles of calcite and dolomite at the beginning (solid lines) and end (dashed lines) of the experiment.

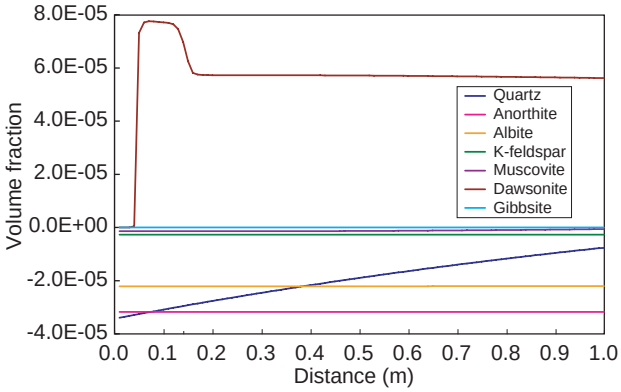

Figure 9

Calculated changes in mineral volumes at the end of the experiment.

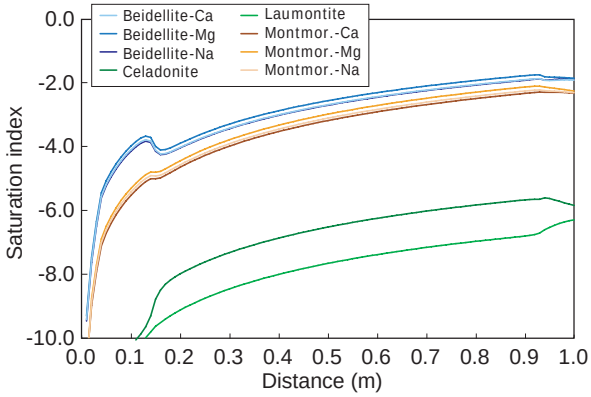

Figure 10

Calculated profiles of saturation index for selected minerals.

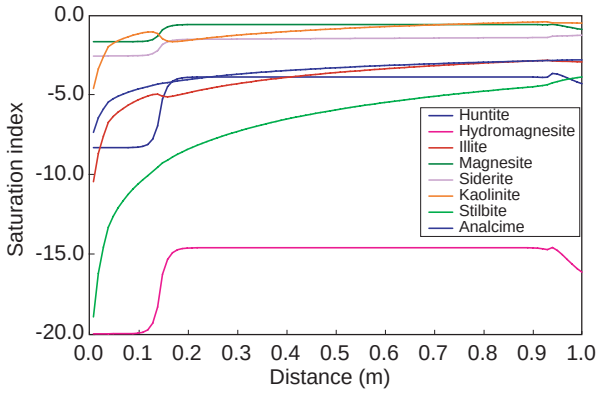

Figure 11

Calculated profiles of saturation index for selected minerals.

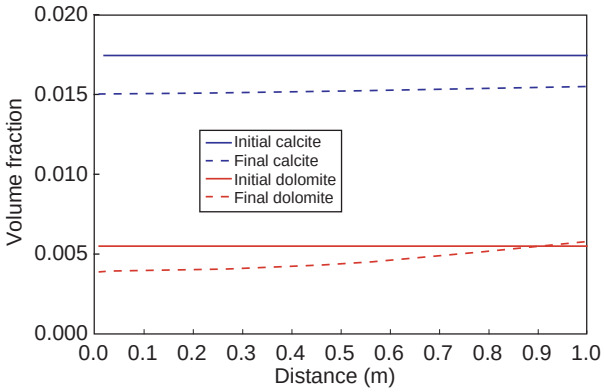

Figure 12

Calculated profiles of calcite and dolomite at the beginning (solid lines) and end (dashed lines) of the experiment assuming reduced reactive surface areas.

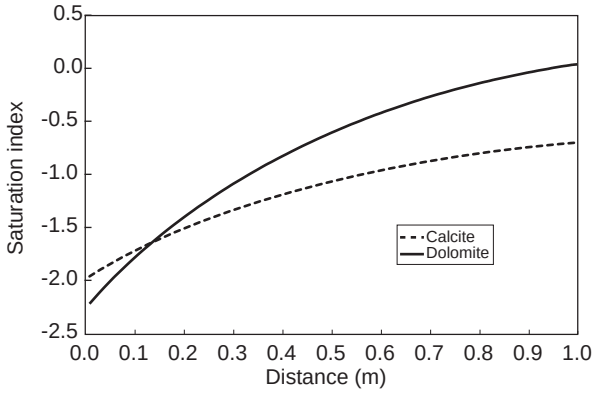

Figure 13

Variation of the modelled saturation index along the column at the end of the experiment.

of the profile with a slight enhancement behind the dolomite dissolution front. The dawsonite is itself predicted to be redissolved with the dissolution front having reached about 5 cm down the column by the end of the experiment. Of the other minerals, quartz is predicted to show a slight differential of dissolution as a function of distance along the column while the dissolution of anorthite and albite are constant along the length of the column.

As indicated above, the model also tracked the saturation state of a number of other potential secondary minerals. Figures 10 and 11 plot the calculated profiles of saturation index along the column at the end of the experiment. It can be seen that all are exhibiting various degrees of undersaturation.

4.5 Additional CO_2 Column Model Calculations

The above calculations were all performed prior to the analysis of both the reactant fluids and the solids. Mineralogical examination of the columns after completion of the experiments showed that the extent of carbonate alteration was much less than the predictive models suggested. In particular, the observations showed that significant corrosion of the calcite and dolomite grains only occurred close to the inlet with minor dissolution effects extending to about 20 cm down the column. Some additional calculations were therefore performed with reduced surface areas to try to improve the correspondence between model and experimental data. It may be noted that the reduction of surface area is exactly equivalent to a reduction of the rate constant, *k*.

Figure 12 shows the changes in carbonate volumes along the column when the surface areas have been reduced by an arbitrary factor of 100 relative to the original calculations.

It can be seen that the dissolution of the carbonates has been greatly reduced so that relatively small changes occur, but these changes occur along the whole length of the column and are not restricted to the vicinity of the inlet end as is seen in the data. Figure 13 shows how the saturation index for calcite and dolomite vary along the column in the model. It can be seen that the calcite is undersaturated by nearly an order of magnitude or more over the whole column whilst the dolomite only comes close to saturation towards the outlet end.

It may be noted that the mineralogical observations would seem to suggest that the CO_2 saturated input fluid comes to equilibrium with the minerals of the column rather quickly, contrary to the result of this calculation. At the same time, the relatively small amount of dissolution seen indicates that the fluid is much closer to saturation than has been assumed for all these models, which may in turn indicate that it is the thermodynamic data that needs to be examined rather than the kinetics.

The concentrations of selected components in the outflow fluid are plotted in Figures 14, 15 and 16. Modelled K and Mg levels seem to be quite close to those observed experimentally whilst the modelled Ca values fall slightly below those measured. The modelled Si concentration is substantially lower than the measured values and show no indication of the peak seen around 1000 h. It may be noted that the surface areas for the silicate minerals were not reduced in this model, only the carbonates areas. If the silicate areas had been reduced too the modelled Si concentrations would have been much lower. Figure 16 shows that the modelled HCO_3^- levels are generally similar to those measured, but the data show a distinct rising trend with time, which is not seen in the model.

Consideration was also given to performing additional calculations incorporating a correction for the CO_2 fugacity. However, this was not performed as it was thought that the correction would lead to lower HCO_3^- levels in the input fluid which would tend to increase the dissolution of carbonates, thereby increasing the discrepancy between the model and the observations.

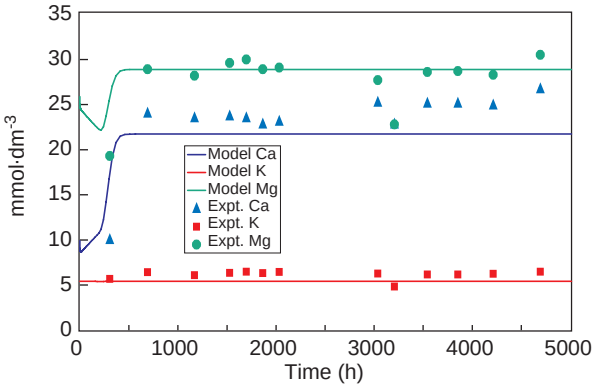

Figure 14

Modelled values of Ca, K, and Mg concentration in the outflow fluid.

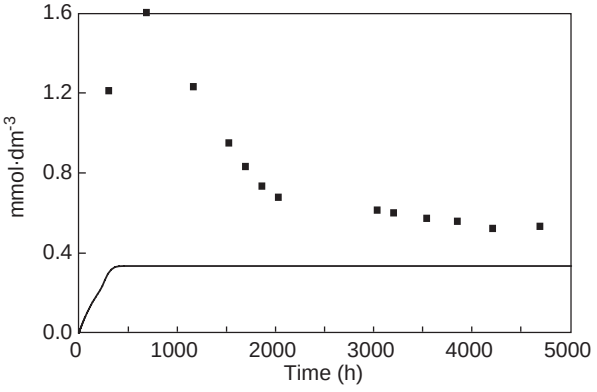

Figure 15

Comparison of modelled values (solid line) of Si concentration in the outflow fluid with the results from the experiment (squares).

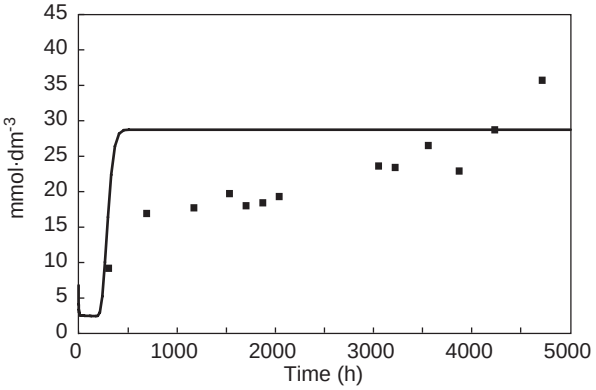

Figure 16

Comparison of modelled values (solid line) HCO_3^- concentration in the outflow fluid with the results form the experiment (squares).

CONCLUSIONS

The aim of this work was to provide a well-constrained long-term laboratory experiment reacting known quantities of minerals with CO_2-rich fluids, order to try and represent situations where CO_2 is being injected into lithologies deep underground. The experimental results have then been used as a test case for predictive geochemical computer modelling.

The experiment, though complex in terms of equipment, was successful in that a run time of approximately 7.5 months was achieved together with the recovery of the intact column from the equipment at the end of the experiment. This column was then examined for mineralogical changes and the collected fluids analysed to provide data on the fate of the dissolved species. However, even with such a long reaction time mineralogical observations have been difficult as the degree of reaction was small. Changes were readily observable on the carbonates present in the starting material, which matches well with the observed trends in the fluid chemistry. However, although changes in silica concentrations were seen in the fluid chemistry no evidence for pitting or etching was noted in the silica bearing phases.

Modelling of the experimental systems was performed using the BGS coupled code, PRECIP prior to the analysis of the reactant fluids and solids with additional calculations performed when the experiment was completed to try to improve the correspondence between model and experimental data. As a general conclusion, the model predictions tend to over estimate the degree of reaction compared with the results from the experiment. In particular, some mineral phases (*e.g.* dawsonite) that are predicted to form in large quantities by the model are not seen at all in the experimental system.

These differences between the model predictions and the experimental observations are not thought to be as a result of the model itself but a are more likely a reflection on the quality of the equilibrium and kinetic constants used for the predictions. Data for the equilibrium constants used here have been taken from EQ36 database data0.com.V8.R6, complied by the *Lawrence Livermore National Laboratory* (United States) and whilst this database is well documented it still only represents a compilation of the best (in the compliers opinion) and in some cases the only data available at the time of compilation and with all such databases needs to be used with caution.

Data for the kinetic constants are more problematic, much of the data used in this study were taken from literature sources. However, these references are mainly concerned with high pH conditions so that some extrapolation has been necessary. In addition, no specific data were available for anorthite, K-feldspar, clinochlore, daphnite, dawsonite, or gibbsite so that it has been necessary to make guesses as to how these minerals behave relative to the better known ones. Finally, it has been found in previous columns studies (Hoch *et al.*, 2002) that literature dissolution rates are commonly too fast to be compatible with the results from such experiments, so some "rounding down" has been applied to the silicate mineral rates.

One key area that the present study highlights is that for modelling to be used as a successful tool to predict the long-term fate of carbon dioxide (CO_2) stored underground, the thermodynamic and kinetic data need to be available under appropriate conditions (pH, and chemical composition of the fluid as well as temperature, and pressure), as extrapolation or "best guesses" may lead to errors being induced in the predictions. Some of these errors and gaps in the data become obvious when comparing the model predictions with experiments which serves to highlight the importance of having "test cases" against which the predictive models can be validated.

ACKNOWLEDGEMENTS

This paper is published with the permission of the Director, *British Geological Survey (NERC)*.

REFERENCES

Brunauer, S, Emmet, P.H. and Teller, E. (1938) Adsorption of Gases in Multimolecular Layers. *Journal of the American Chemical Society*, **60**, 309-319.

Brady, P.V. and J.V. Walther, (1989). Controls on silicate dissolution rates in neutral and basic pH solutions at 25°C. *Geochimica et Cosmochimica Acta*, **53**, 2823-2830.

Brady, P.V. and J.V. Walther, (1990). Kinetics of Quartz Dissolution at Low Temperature, *Chemical Geology*, **82**, 253-264.

Helgeson, H.C., Murphy, W.M. and Aagaard, P., (1984). Thermodynamics and kinetic constraints on reaction rates among minerals and aqueous solutions – II. Rate constraints, effective surface area, and the hydrolysis of feldspar. *Geochimica et Cosmochimica Acta*, 48, 2405-2432.

Hoch, A.R., Linklater, C.M., Noy, D.J., and Rodwell, W.R. (2002) Nagra/Nirex/SKB Column Experiments: A Further Geochemical Modelling Study. *SERCO Report ECOCLA*Y II/02/N1.

Knauss, K.G. and T.J. Wolery (1986) Dependence of Albite Dissolution Kinetics on pH and Time at 25°C and 70°C, *Geochimica et Cosmochimica Acta*, **50**, 2481-2497.

Knauss, K.G. and T.J. Wolery (1988) The Dissolution Kinetics of Quartz as a Function of pH and Time at 70°C, *Geochimica et Cosmochimica Acta*, **52**, 43-53.

Knauss, K.G. and T.J. Wolery (1989) Muscovite Dissolution Kinetics as a Function of pH and Time at 70°C, *Geochimica et Cosmochimica Acta*, **53**, 1493-1501.

Noy D.J. (1998) User guide to PRECIP, a program for coupled groundwater flow and reactive solute transport. *British Geological Survey Technical Report* WE/98/13. British Geological Survey, Keyworth. UK.

Parkhurst, D.L. and Appelo, C.A.J. (1999) User's guide to PHREEQC (version 2) – a computer program for speciation, reaction-path, 1D-transport, and inverse geochemical calculations. *US Geol. Surv. Water Resour. Inv. Rep. 99-4259*,

Pearce, J.M., Czernichowski-Lauriol, I., Rochelle, C.A., Springer, N., Brosse, E., Sanjuan, B., Bateman, K. and Lanini, S. (2000) How will reservoir and caprock react with injected CO_2 at Sleipner? Preliminary evidence from experimental investigations. *Proceedings of the 5th International Conference on Greenhouse Gas Control Technologies (GHGT-5)*, Cairns, Queensland, Australia.

Savage, D., Noy D., Miharac M. (2002) Modelling the interaction of bentonite with hyperalkaline fluids. *Applied Geochemistry*, **17**, 207–223.

Final manuscript received in December 2004